DOI: 10.1002/ejic.200600889

Intra- and Intermolecular H···Cl–Ni Bonding Patterns in a Series of Highly Preorganized Dinuclear Nickel(II) Complexes

Feng-Mei Nie,[a][‡] Guido Leibeling,[a] Serhiy Demeshko,[a] Sebastian Dechert,[a] and Franc Meyer*[a]

Keywords: Nickel / Dimetallic complexes / Hydrogen bonds / Pyrazolate ligands / Magnetic properties

Four dinickel complexes $[L^1Ni_2(\mu\text{-}Cl)(Cl)_2]\cdot 2CH_3OH$ (**1a**), $[L^1Ni_2(\mu\text{-}Cl)(CH_3OH)](ClO_4)_2$ (**1b**), $[L^2Ni_2(\mu\text{-}Cl)Cl_2(H_2O)_2]\cdot H_2O$ (**2**) and $[L^3Ni_2Cl_2(CH_3OH)_2]Cl\cdot 2CH_3OH$ (**3**) were synthesized and structurally characterized. The ligand scaffolds have a central pyrazolato bridge and N-donor chelate arms that provide two proximate binding pockets for the nickel ions. While the longer ligand side arms in **1a**, **1b** and **2** induce Ni···Ni distances of around 4.0 Å and favour incorporation of a chlorido bridge within the dimetallic pocket, a stretched Ni···Ni separation of 4.6 Å with an unusual intramolecular Cl···H–O linkage is observed in **3**. Various Cl···H–O hydrogen-bonding motifs are identified in the solid-state structures of **1**–**3**, where either the H-donor (MeOH or H_2O) or the H-acceptor (chlorido) or both are bound to a nickel ion, and their relative donor–acceptor distances are discussed. Magnetic coupling mediated through the pyrazolato and chlorido bridges is rather weak and antiferromagnetic, but it is even weaker for the Cl···H–O linkage.

Introduction

Hydrogen bonding to metal-bound ligands can have profound effects on fundamental properties of the metal complex, such as the metal–ligand bond lengths, redox potentials and reactivity.[1–3] Metal-bound chlorido ligands have been identified as a very good hydrogen-bond acceptor (in contrast to its organochlorine counterpart), having the potential to interact with hydrogen-bond donors in both a strong (i.e., short) and anisotropic fashion.[4,5] While hydrogen bonds to metal-bound fluorido ligands are even stronger, they also exhibit a distinct angular preference for larger H···F–M angles.[6] Intermolecular D–H···X–M (D = N, O; X = F, Cl, Br, I) interactions are increasingly applied in molecular recognition, crystal engineering and the noncovalent assembly of metallosupramolecules,[7,8] while intramolecular D–H···X–M motifs involving pendant nonligating hydrogen-bonding groups allow the stabilization of unusual ligands, such as HF, at a metal ion.[9] A particular situation arises if the hydrogen-bond donor D is itself acting as a ligand towards a second metal ion. This may enhance the acidity of the D–H unit and may induce particularly strong intramolecular D–H···X–M interactions, as was observed in some Cu–(H)O–H···F–Cu motifs with extremely short H···F distances.[10,11] In order to enforce the formation of such hydrogen bonds, the use of dinucleating ligand scaffolds that constrain the metal–metal separation appears most promising. Here we report the structural characterization of a series of pyrazolato-based dinickel chloride complexes that exhibit various hydrogen-bonding arrangements. These involve the nickel-bound chlorido ligand and water or methanol solvent molecules, comprising an unusual intramolecular Ni–(Me)O–H···Cl–Ni interaction. The set of compartmental ligands used in this work is depicted in Scheme 1.

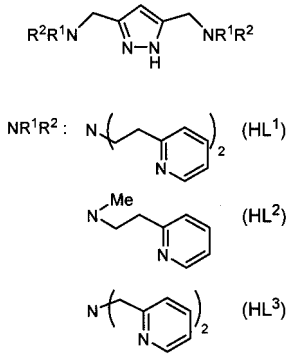

Scheme 1. Ligands used in this work.[10]

The ligands differ by the number of side arm donor sites (HL^1 versus HL^2) or by the side arm chain length (HL^1 versus HL^3). The latter variation was previously shown to determine the preferred metal–metal distance in the resulting dimetallic complexes, with the shorter side arms in

[a] Institut für Anorganische Chemie, Georg-August-Universität Göttingen
Tammannstrasse 4, 37077 Göttingen, Germany
Fax: +49-551-393063
E-mail: franc.meyer@chemie.uni-goettingen.de
[‡] New address: Department of Chemistry, Capital Normal University,
Beijing 100037, P. R. China
Supporting information for this article is available on the WWW under http://www.eurjic.org or from the author.

HL^3 enforcing larger metal–metal distances of >4 Å.[12,13] With 3d transition-metal ions such as copper(II) and zinc(II), $\{L^1M_2\}$ scaffolds (M = Cu, Zn) allow small bridges such as a hydroxido group to span the two metal ions, while the shorter ligand side arms in $\{L^3M_2\}$ pull the metal ions back and apart. The latter situation induces incorporation of an additional solvent molecule, giving functionalities such as (H)O–H–O(H) or F–H–O(H) within the dimetallic pocket.[10,14] Similar effects are now anticipated in nickel complexes of the current pyrazolato ligands and are investigated in order to probe hydrogen-bonding patterns to nickel-bound chlorido ligands.

Results and Discussion

Synthesis and Structural Characterization

Dinickel complexes of $[L^1]^-$, $[L^2]^-$ and $[L^3]^-$ were readily prepared from the respective pyrazole derivative HL^1, HL^2 and HL^3, 2 equiv. of $NiCl_2{\cdot}6H_2O$ and a base (usually NEt_3). Crystalline material of the resulting complexes **1a**, **2** and **3** was obtained from methanol/diethyl ether solutions. In order to gain some insight into the structural consequences that result from the presence of fewer chlorido ligands, complex **1b** was prepared by a similar procedure starting from HL^1, but using 2 equiv. of $Ni(ClO_4)_2{\cdot}6H_2O$ and 1 equiv. of NaCl. FAB mass spectra of **1a**, **2** and **3** feature dominant signals for the respective $[LNi_2Cl_2]^+$ ions, while the FAB mass spectrum of **1b** shows a signal for $[L^1Ni_2Cl(ClO_4)]^+$.

The molecular structures of all four complexes are depicted in Figures 1, 2, 3 and 4, along with selected interatomic distances and bond angles. In all cases the two nickel ions are hosted within the binding pockets of the ligand scaffold, spanned by the pyrazolato ligand and coordinated by the side arm nitrogen atoms. In $[L^1Ni_2Cl_3]$ (**1a**), both nickel(II) ions are six-coordinate; the coordination environment of each nickel ion consists of four nitrogen atoms from the pyrazolato, a bridging chlorido and a terminal chlorido ligand (Figure 1). Interestingly, the chlorido ligand at Ni1 is located *trans* to the pyrazolato N1 atom, while the chlorido ligand at Ni2 is found *trans* to the pyridyl N8 atom. When only a single chlorido ligand is present per dimetallic entity in $[L^1Ni_2(Cl)(CH_3OH)](ClO_4)_2$ (**1b**), it occupies the bridging position, leaving Ni2 five-coordinate while a methanol solvent molecule fills the remaining site at Ni1 (Figure 2). Fewer ligand side arms in $[L^2Ni_2Cl_3(H_2O)_2]$ (**2**) allow for the binding of a water solvent molecule to each of the metal ions, with one of the chlorido ligands in the bridging position and the others terminally bound *trans* to the pyrazolato N atom (Figure 3). The Ni–O distances in **1b** and **2** (2.16 and 2.14 Å) are comparable to those found in other six-coordinate nickel complexes with three or four nitrogen donor atoms and one or two chlorido ligands, as for example in $[(phen)_2NiCl(H_2O)]Cl{\cdot}EtOH{\cdot}H_2O$ (2.03 Å, phen = 1,10-phenanthroline)[15] or [(1,4,8,11-tetraazaundecane)$NiCl(H_2O)$]Cl (2.18 Å).[16] Metal···metal separations in all three complexes are very similar and quite short at 4.09 (**1a**), 4.00 (**1b**) and 4.11 (**2**) Å. It should be noted that related nickel(II) chloride complexes of some pyrazolato-derived ligands bearing aliphatic N-donor side arms usually feature five-coordinate nickel atoms,[17] in contrast to the systems studied here. However, close inspection reveals that the Ni–Cl–Ni bridge in **1a** is highly asymmetric with a long Ni1–Cl2 distance (2.82 Å) and a much shorter Ni2–Cl2 bond (2.50 Å). All other Ni–Cl distances ranging from 2.36 to 2.57 Å for Ni–Cl and from 2.46 to 2.65 Å for Ni–(μ-Cl) are in agreement with expectations.[17] The slight asymmetry of the Ni–Cl–Ni bridge in **1b** [*d*(Ni1–Cl1) = 2.61 Å, *d*(Ni2–Cl1) = 2.46 Å] reflects the different coordination numbers of the metal ions. The methanol molecule bound to Ni1 in **1b** is hydrogen-bonded to one of the perchlorate counteranions [*d*(O1···O21) = 2.80 Å].

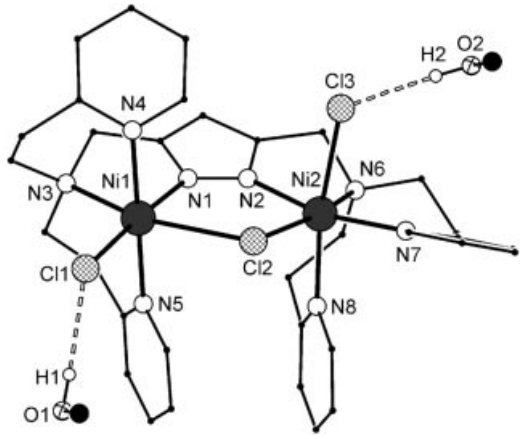

Figure 1. Plot of the molecular structure of **1a**. All hydrogen atoms except the O–H protons have been omitted for clarity. Selected interatomic distances [Å] and angles [°]: Ni1–Cl1 2.3632(6), Ni1–Cl2 2.8251(6), Ni1–N1 1.982(2), Ni1–N3 2.180(2), Ni1–N4 2.142(2), Ni1–N5 2.117(2), Ni2–Cl2 2.4947(5), Ni2–Cl3 2.5723(6), Ni2–N2 1.984(2), Ni2–N6 2.205(2), Ni2–N7 2.105(2), Ni2–N8 2.118(2), Ni1···Ni2 4.0917(6), O1–H1 0.86(3), O1···Cl1 3.184(2), O2–H2 0.82(3), O2···Cl3 3.062(2); Ni1–Cl2–Ni2 100.37(2), N1–Ni1–Cl1 175.94(4), N1–Ni1–Cl2 82.25(4), Cl2–Ni1–N3 162.44(4), N4–Ni1–N5 178.30(6), N2–Ni2–N7 166.14(6), N2–Ni2–Cl2 87.73(4), Cl3–Ni2–N8 169.42(4), O1–H1···Cl1 162(3), O2–H2···Cl3 170(3).

The terminal chlorido ligands in **1a** are involved in hydrogen bonding with methanol molecules included in the crystal lattice (Figure 1), where the Cl···O distances correlate with the Ni–Cl bond lengths; the chlorido ligand Cl1 with a short *d*(Ni1–Cl1) = 2.36 Å forms a relatively long hydrogen bond [*d*(Cl1···O1) = 3.18 Å], while the hydrogen bond of the more loosely bound Cl3 [*d*(Ni2–Cl3) = 2.57 Å] is significantly shorter at *d*(Cl3···O2) = 3.06 Å. The pyrazolato-based dinickel entities in **2** are strongly dimerized in the solid state through a series of O–H···Cl hydrogen bonds (Figure 3). In this closed hydrogen-bonding motif each nickel-bound water molecule forms two hydrogen bonds to chlorido ligands of the opposite dinickel array, giving rise to a zig-zag sequence of O–H···Cl linkages. The dimerized

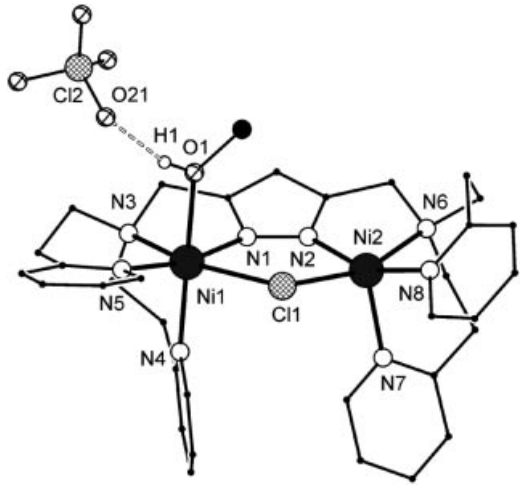

Figure 2. Plot of the molecular structure of **1b**. All hydrogen atoms except the O–H protons and the second ClO_4^- ion have been omitted for clarity. Selected interatomic distances [Å] and angles [°]: Ni1–Cl1 2.610(1), Ni1–O1 2.162(3), Ni1–N1 1.975(3), Ni1–N3 2.138(3), Ni1–N4 2.095(3), Ni1–N5 2.084(3), Ni2–Cl1 2.455(1), Ni2–N2 1.944(3), Ni2–N6 2.157(4), Ni2–N7 2.043(3), Ni2–N8 2.039(4), Ni1···Ni2 4.0038(8), O1–H1 0.82(1), O1···O21 2.803(4); Ni1–Cl1–Ni2 104.43(4), N1–Ni1–N5 167.7(1), N1–Ni1–Cl1 82.9(1), Cl1–Ni1–N3 162.97(9), O1–Ni1–N4 175.3(1), N2–Ni2–N8 156.8(2), N2–Ni2–Cl1 87.0(1), Cl1–Ni2–N6 161.2(1), Cl1–Ni2–N7 99.3(1), O1–H1···O21 164(5).

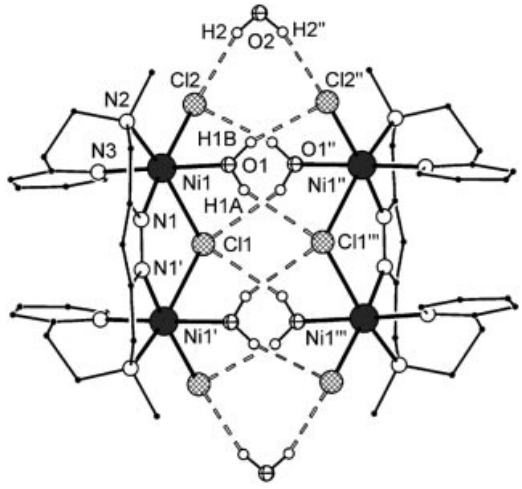

Figure 3. Plot of the molecular structure of **2**. All hydrogen atoms except the O–H protons have been omitted for clarity. Selected interatomic distances [Å] and angles [°]: Ni1–Cl1 2.6447(5), Ni1–Cl2 2.4013(5), Ni1–O1 2.143(1), Ni1–N1 1.996(2), Ni1–N2 2.148(2), Ni1–N3 2.080(2), Ni1···Ni1′ 4.1119(5), Ni1···Ni1′′ 5.4022(6), Ni1···Ni1′′′ 6.7890(5), O1–H1A 0.80(3), O1···Cl1′′′ 3.286(2), O1–H1B 0.86(3), O1···Cl2′′ 3.145(2); O2–H2 0.87(2), O2···Cl2 3.249(2), Ni1–Cl1–Ni1′ 102.04(2), N1–Ni1–Cl2 173.35(5), N1–Ni1–Cl1 83.96(5), Cl1–Ni1–N2 163.41(4), O1–Ni1–N3 177.98(6), O1–H1A···Cl1′′′ 155(3), O1–H1B···Cl2′′ 161(2), O2–H2···Cl2 163(4). Symmetry transformations used to generate equivalent atoms: ′: x, $1-y$, z; ′′: $1-x$, y, $2-z$; ′′′: $1-x$, $1-y$, $2-z$.

arrangement is capped by hydrogen bonds to two additional water molecules included in the crystal lattice, thus preventing the formation of chains or 3D hydrogen-bonded

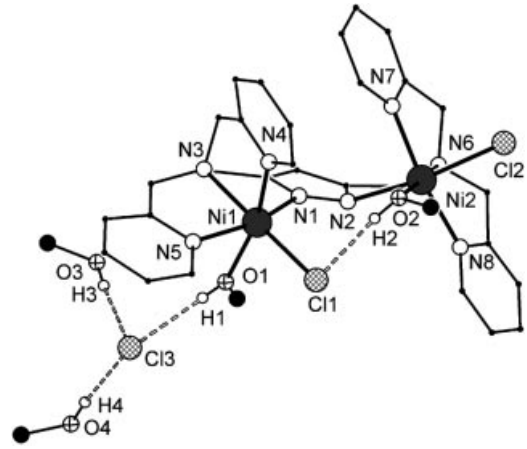

Figure 4. Plot of the molecular structure of **3**. All hydrogen atoms except the O–H protons have been omitted for clarity. Selected interatomic distances [Å] and angles [°]: Ni1–Cl1 2.3641(6), Ni1–O1 2.184(2), Ni1–N1 2.052(2), Ni1–N3 2.121(2), Ni1–N4 2.092(2), Ni1–N5 2.082(2), Ni2–Cl2 2.4522(7), Ni2–O2 2.070(2), Ni2–N2 2.144(2), Ni2–N6 2.106(2), Ni2–N7 2.066(2), Ni2–N8 2.070(2), Ni1···Ni2 4.6007(7), O1–H1 0.77(3), O1···Cl3 3.054(2), O2–H2 0.83(3), O2···Cl1 3.052(2), O3–H3 0.80(3), O3···Cl3 3.150(2), O4–H4 0.85(4), O4···Cl3 3.133(2); N1–Ni1–N5 159.32(6), N1–Ni1–Cl1 101.35(4), Cl1–Ni1–N3 177.81(5), O1–Ni1–N4 166.58(6), N2–Ni2–Cl2 171.67(4), N2–Ni2–O2 91.82(6), O2–Ni2–N6 174.73(6), N7–Ni2–N8 161.91(7), O1–H1···Cl3 167(3), O2–H2···Cl1 172(3), O3–H3···Cl3 174(3), O4–H4···Cl3 174(3).

networks. Overall, each chlorido ligand and each water molecule is involved in two hydrogen-bonding contacts. The resulting dimer of dinickel subunits in **2** is located on a centre of inversion, with each dinickel molecule having crystallographically imposed C_s symmetry. As expected, O–H···Cl interactions to the bridging chlorido ligands are the longest at d(Cl1···O1) = 3.29 Å, but they are well within the range expected for HOH···Cl or RCH_2OH···Cl hydrogen bonds.[5,8]

The molecular structure of **3** that incorporates the pyrazolato ligand $[L^3]^-$ with shorter side arms differs fundamentally from those of **1a**, **1b** and **2**, since the chlorido atom Cl1 does not occupy a bridging position within the dimetallic pocket (Figure 4). Instead, a methanol molecule is inserted at Ni2 to give an unusual intramolecular Ni–Cl···H–O(Me)–Ni bridge with a short hydrogen bond [d(Cl1···O2) = 3.05 Å]. As a consequence, the Ni···Ni separation in **3** (4.60 Å) is considerably longer than in **1a**, **1b** and **2** (4.09, 4.00 and 4.11 Å, respectively). Ligand $[L^3]^-$ has previously been shown to favour longer metal–metal separations of around 4.5 Å because of the shorter chelate arms than those of $[L^1]^-$.[12] Observation of $[L^3Ni_2Cl_2]^+$ as the dominant ion in the FAB mass spectrum of **3** suggests, however, that the inserted methanol molecule is readily lost under reduced pressure.

Both nickel(II) ions in **3** are six-coordinate, but a major difference to the analogous complex of ligand $[L^1]^-$ (i.e., complex **1a**) is the coordination isomerism of some chlorido

ligands. In **1a** a chlorido ligand (Cl1) is terminally bound to Ni1 and forms a hydrogen bond to a lattice methanol molecule, while an inverse situation is found for **3** where the methanol molecule acts as a ligand to Ni1 and is hydrogen-bonded to the chlorido ligand Cl3 that is dissociated from the metal ion. The distance Cl3···O1 in **3** is very short and comparable to the short intramolecular Cl···H–O linkage (3.05 Å), in accordance with the idea that a dissociated chloride ion should be a better H-bond acceptor because of its larger negative charge compared with a metal-bound chlorido ligand such as in **1a** and **2**.[5] Interestingly, the "free" Cl3 in **3** forms two further hydrogen-bonding interactions to lattice methanol molecules which are significantly longer (3.13 and 3.15 Å; Figure 4) than the hydrogen bond to nickel-bound O1, thus supporting the assumption that the hydrogen-bond strength is enhanced by coordination and acidification of the H-donor methanol.

Magnetic Properties

In order to evaluate the effect of the different structural features and bridging units of the dimetallic scaffolds on the magnetic coupling between the proximate nickel(II) (S = 1) ions, magnetic susceptibility measurements were carried out for all four complexes at two different magnetic fields in a temperature range from 2.0 to 295 K. No significant field dependence was observed for any of the complexes. The temperature dependence of the magnetic susceptibility χ_M and the product $\chi_M T$ is shown in Figure 5. In all cases, the observed $\chi_M T$ values of around 2.5 $cm^3 K mol^{-1}$ (≈ 4.5 μ_B) at room temperature are close to the value expected for two uncoupled nickel(II) ions ($\chi_M T$ = 2.42 $cm^3 K mol^{-1}$ for g = 2.2). The $\chi_M T$ curves gradually but steadily drop with decreasing temperature and finally tend to zero, indicating an S = 0 ground state. χ_M accordingly goes through a maximum, but only at very low temperatures, suggesting that the coupling is weak.

Magnetic parameters were determined using a fitting procedure to the appropriate Heisenberg spin Hamiltonian for isotropic exchange coupling. Simulation of the experimental magnetic data was performed with full-matrix diagonalization of exchange coupling and Zeeman splitting according to the Hamiltonian in Equation (1).[18]

$$H = -2J\vec{S}_1\vec{S}_2 + g\mu_B(\vec{S}_1 + \vec{S}_2)\vec{B} \quad (1)$$

Before simulation the experimental data were corrected for the underlying diamagnetism by using tabulated Pascal constants (incremental method) and for temperature-independent paramagnetism (*TIP*; included in the data representation in Figure 5). A Curie-behaved paramagnetic impurity (*PI*) with spin S = 1 was included according to $\chi = (1 - PI)\chi + PI\chi_{mono}$. Satisfactory fits were obtained for all four systems, and values for g, J, *PI* and *TIP* are listed in Table 1.

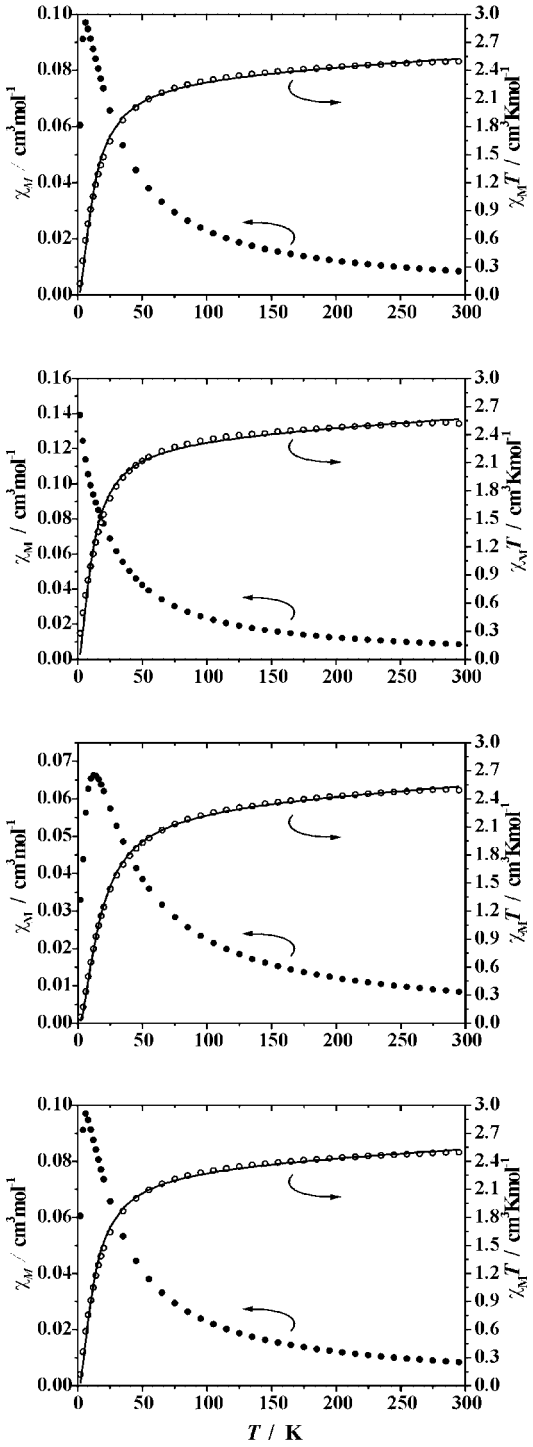

Figure 5. χ_M (solid circles) and $\chi_M T$ (open circles) vs. T plot for **1a** (top), **1b** (second from top), **2** (second from bottom) and **3** (bottom) at 5000 G; the solid line represents the calculated curve fit (see text).

Table 1. Magnetic parameters for complexes **1a**, **1b**, **2** and **3** according to Equation (1).

	1a	**1b**	**2**	**3**
g	2.18	2.20	2.22	2.20
J [cm^{-1}]	–3.6	–3.4	–5.1	–1.7
PI [%]	0.7	2.0 (fixed)	2.0 (fixed)	1.5
TIP [10^{-4} $cm^3 mol^{-1}$]	7.2	7.8	7.8	4.3

Since nickel(II) may exhibit significant zero-field splitting that can be similar in magnitude to the *J* values determined, data analysis was also probed with an additional term $2D[S_z^2 - 1/3S(S + 1)]$ included in Equation (1) that accounts for a local zero-field splitting parameter *D*. However, with reasonable values for *D* and *PI* this analysis did not lead to any substantial changes in the *J* values, while the decrease of $\chi_M T$ at low temperatures could not be described by considering *D* only (i.e., without exchange Hamiltonian, $J = 0$).[19]

In view of the aggregation of **2** in the solid state as described earlier, an alternative "dimer of dimer" model according to Scheme 2 has also been applied to the magnetic data analysis of this complex. This model gives a similarly good fit with $g = 2.25$, $J_1 = -3.9\ cm^{-1}$, $J_2 = -2.6\ cm^{-1}$, $PI = 2\%$ and $TIP = 8.8 \times 10^{-4}\ cm^3 mol^{-1}$. Note that assignment of J_1 and J_2 to the *intra*dimer and *inter*dimer coupling is arbitrary because of the symmetry of the Hamiltonian.

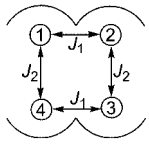

Scheme 2. Alternative coupling scheme for **2**.

Rather small negative *J* values confirm relatively weak antiferromagnetic coupling between the adjacent nickel ions in all cases, but subtle differences are discernible. The coupling is clearly weakest in **3**, while it appears to be strongest in **2**. Although the multitude of structural variations among the four complexes (coordination numbers and geometries, distortion of the nickel ions out of the pyrazolato plane, etc.) prevents any definite interpretation in terms of magnetostructural correlations, one may attribute the much lower *J* value for **3** to the lack of a chlorido bridge and to the much weaker coupling efficiency of the intramolecular Cl···H–O linkage. This also corroborates the assignment of J_1 and J_2 in the "dimer of dimer" model for **2**, since any interaction through the hydrogen bonds should be weak. The somewhat weaker coupling in **1a** and **1b** relative to the coupling within the pyrazolato-based dinickel entities of **2** may be a result of the pronounced asymmetry of the Ni–Cl–Ni bridge and the presence of a very long Ni–Cl bond in the two former systems [*d*(Ni1–Cl2) = 2.83 Å in **1a**; *d*(Ni1–Cl1) = 2.61 Å in **1b**], as such long distances provide no efficient exchange pathway. It should be emphasized, though, that additional factors such as the canting between the basal planes of the two nickel ions and the plane of the pyrazolato bridge will also play a substantial role and should contribute to the diminished coupling in **3**.

Conclusions

The compartmental pyrazolato-based ligands HL^1, HL^2 and HL^3 with pyridyl side arms are obviously well suited to form dinuclear nickel(II) complexes, similar to related pyrazolato ligands with aliphatic chelate arms. Since the latter have provided useful scaffolds for synthetic models of the active site of the dinickel enzyme urease, a likewise rich chemistry is now expected for HL^1, HL^2 and HL^3. The current set of complexes confirms that different Ni···Ni distances and distinct coordination spheres can be obtained by proper modifications of the ligand side arms attached to the central pyrazolato bridge. Various O–H···Cl hydrogen-bonding motifs were characterized crystallographically in **1**–**3**, where either the H-donor (MeOH or H_2O) or the H-acceptor (chlorido) or both are bound to a metal ion, that is, nickel(II). The structural trends are in line with the following ranking of such interactions: (1) the hydrogen bond is shortened by coordination and acidification of the H-donor, *d*[Cl⁻···H(Me)O–Ni] < *d*[Cl⁻···H(Me)O]; (2) free chloride ions are better H-acceptors than metal-bound chlorido ligands, *d*[Cl⁻···H(Me)O–Ni] < *d*[Ni–Cl···H(Me)-O–Ni]; and (3) a terminal chlorido ligand is a better H-acceptor than a bridging one, *d*[Ni–Cl···H(H)O–Ni] < *d*[Ni(μ-Cl)···H(H)O–Ni]. Magnetic couplings through the chlorido and pyrazolato bridges are rather weak, but are even weaker through a Cl···H–O linkage or when the metal ions are displaced out of the plane of the pyrazolato ligand. These comparisons may prove useful for the assessment of hydrogen-bonding interactions in molecular recognition, crystal engineering and related fields.

Experimental Section

Caution! Although no problems were encountered in this work, transition metal perchlorates are potentially explosive and should be handled with care and with proper precautions.

General: Ligands HL^1, HL^2 and HL^3 were prepared as described previously.[10] All other chemicals were purchased from commercial sources and used as received. Microanalyses were performed by the Analytical Laboratory of the Inorganic Chemistry Institute at Georg-August-University Göttingen. Infrared spectra: Digilab Excalibur, recorded as KBr pellets. Mass spectra (FAB MS): Finnigan MAT 95 with nitrobenzylalcohol as the matrix.

Synthesis of $[L^1Ni_2(\mu\text{-}Cl)(Cl)_2]\cdot 2CH_3OH$ (1a): A solution of HL^1 (0.273 g, 0.5 mmol) in methanol (40 mL) was treated with 1 equiv. of NEt_3 (0.051 g, 0.5 mmol) and stirred for 10 min. To the reaction mixture was then added a solution of $NiCl_2\cdot 6H_2O$ (0.291 g, 1.0 mmol) in methanol (40 mL), and stirring was continued for a further 2 h. All volatile material was then evaporated under reduced pressure, the residue was taken up in methanol (10 mL) and this solution was filtered. The filtrate was layered with diethyl ether to gradually yield green crystals (203 mg, 49%) of **1a**. $C_{33}H_{37}Cl_3N_8Ni_2\cdot 2CH_3OH$ (833.5): calcd. C 50.43, H 5.44, N 13.44; found C 49.61, H 5.47, N 13.22. FAB MS: *m/z* (%) = 733 (100) $[L^1Ni_2Cl_2]^+$, 698 (60) $[L^1Ni_2Cl]^+$. IR (KBr): $\tilde{\nu}$ = 3474 (s), 3415 (s), 3267 (s), 2853 (m), 1637 (m), 1606 (s), 1567 (m), 1485 (s), 1443 (s), 1330 (s), 1314 (s), 1161 (w), 1108 (w), 1066 (w), 1045 (w), 1021 (m), 939 (w), 785 (s), 758 (s), 582 (w), 422 (w) cm^{-1}.

Synthesis of $[L^1Ni_2(\mu\text{-}Cl)(CH_3OH)](ClO_4)_2$ (1b): A solution of HL^1 (0.273 g, 0.5 mmol) in methanol (40 mL) was treated with 1 equiv. of NEt_3 (0.051 g, 0.5 mmol) and stirred for 10 min. The reaction mixture was then transferred to a solution containing 2 equiv. of $Ni(ClO_4)_2\cdot 6H_2O$ (0.365 g, 1.0 mmol) in methanol (40 mL). The re-

action mixture was stirred for 1 h before 1 equiv. of NaCl (0.027 g, 0.5 mmol) was added, and stirring was continued overnight. All volatile material was then evaporated under reduced pressure, the residue was taken up in methanol (10 mL) and the solution was filtered. The filtrate was layered with diethyl ether to gradually yield green crystals (139 mg, 29%) of **1b**. $C_{34}H_{41}Cl_3N_8Ni_2O_9$ (929.5): calcd. C 43.94, H 4.45, N 12.06; found C 43.81, H 4.57, N 11.93. FAB MS: *m*/*z* (%) = 797 (100) $[L^1Ni_2Cl(ClO_4)]^+$, 696 (30) $[L^1Ni_2Cl]^+$. IR (KBr): $\tilde{\nu}$ = 3410 (m), 3074 (w), 2939 (w), 2902 (w), 2858 (w), 1609 (s), 1568 (m), 1488 (s), 1443 (s), 1383 (w), 1336 (w), 1310 (m), 1296 (w), 1162 (m), 1088 (vs), 1020 (s), 981 (m), 933 (m), 831 (w), 781 (m), 765 (m), 646 (w), 623 (s), 587 (w), 462 (w), 424 (m) cm^{-1}.

Synthesis of $[L^2Ni_2(\mu\text{-}Cl)Cl_2(H_2O)_2]\cdot H_2O$ (2): A solution of HL^2 (0.181 g, 0.5 mmol) in methanol (40 mL) was treated with 1 equiv. of NEt_3 (0.051 g, 0.5 mmol) and stirred for 10 min. The reaction mixture was then transferred to a solution containing 2 equiv. of $NiCl_2\cdot 6H_2O$ (0.291 g, 1.0 mmol) in methanol (40 mL) and stirred for a further 2 h. All volatile material was then evaporated under reduced pressure, the residue was taken up in methanol (10 mL) and the solution was filtered. The filtrate was layered with diethyl ether to gradually yield green crystals (0.103 g, 40%) of **2**. $C_{21}H_{33}Cl_3N_6Ni_2O_3$ (641.3): calcd. C 39.33, H 5.19, N 13.10; found C 38.99, H 5.28, N 12.69. FAB MS: *m*/*z* (%) = 551 (100) $[L^2Ni_2Cl_2]^+$. IR (KBr): $\tilde{\nu}$ = 3379 (br s), 2914 (w), 2859 (w), 2814 (w), 1632 (m), 1607 (s), 1571 (m), 1485 (m), 1444 (s), 1376 (w), 1322 (s), 1287 (w), 1246 (w), 1156 (w), 1099 (w), 1042 (m), 988 (m), 926 (w), 863 (w), 766 (s), 642 (m), 593 (m), 426 (m) cm^{-1}.

Synthesis of $[L^3Ni_2Cl_2(CH_3OH)_2]Cl\cdot 2CH_3OH$ (3): To a solution of $NiCl_2\cdot 6H_2O$ (0.291 g, 1.0 mmol) in methanol (40 mL) was added a solution of HL^3 (0.245 g, 0.5 mmol) and NEt_3 (0.051 g, 0.5 mmol) in methanol (40 mL), and the reaction mixture stirred at room temp. for 2 h. All volatile material was then evaporated under reduced pressure, the residue was taken up in methanol (10 mL) and this solution was filtered. The filtrate was layered with diethyl ether to gradually yield blue needle-like crystals (268 mg, 64%) of **3**. Upon storage in air, the methanol solvent molecules appear to be partly replaced by water, and the compound appears to be somewhat hygroscopic according to elemental analysis. $C_{31}H_{37}Cl_3N_8Ni_2O_2\cdot 4H_2O$ (849.49): calcd. C 43.83, H 5.34, N 13.19; found C 43.32, H 5.08, N 13.02. FAB MS: *m*/*z* (%) = 677 (100) $[L^3Ni_2Cl_2]^+$, 642 (20) $[L^3Ni_2Cl]^+$. IR (KBr): $\tilde{\nu}$ = 3344 (vs), 2920 (w), 1625 (m), 1605 (vs), 1573 (w), 1480 (m), 1441 (s), 1322 (m), 1287 (m), 1259 (w), 1154 (w), 1098 (m), 1052 (w), 1022 (m), 903 (w), 959 (w), 876 (w), 767 (s), 642 (w), 493 (w), 428 (w) cm^{-1}.

X-ray Crystallographic Study: X-ray data for **1a** and **3** were collected with a Bruker P4 diffractometer (graphite-monochromated Mo-K_α radiation, λ = 0.71073 Å) by use of ω scans at –140 °C and –100 °C, respectively (Table 2). Data for **1b** and **2** were collected with a STOE IPDS II diffractometer (graphite-monochromated Mo-K_α radiation, λ = 0.71073 Å) by use of ω scans at –140 °C (Table 2). The structures were solved by direct methods and refined on F^2 using all reflections with SHELX-97.[20] The non-hydrogen atoms were refined anisotropically. Hydrogen atoms which were not involved in hydrogen bonding were placed in calculated positions and assigned to an isotropic displacement parameter of 0.08 $Å^2$. The positional and isotropic thermal parameters of the oxygen-bound hydrogen atoms H1 and H2 in **1a**, H1A/B in **2** and H1 to H4 in **3** were refined without any restraints or constraints. A DFIX restraint (d_{O-H} = 0.82 Å) was applied for the O2–H2 distance in **2**. All other positional and isotropic thermal parameters of the hydrogen atom H2 were refined without restraints or constraints. SADABS was used to perform area-detector scaling and absorption corrections for **1a** and **3**.[21] Face-indexed absorption corrections were performed numerically with the program X-RED for **1b** and **2**.[22] Three oxygen atoms of one ClO_4^- ion in **1b** are disordered about two positions [occupancy factors: 0.852(4)/0.148(4)]. SADI (d_{Cl-O} and $d_{O\cdots O}$) restraints and EADP constraints were used to model the disorder and for anisotropic refinement. CCDC-616755 (**1a**), -616756 (**1b**), -616757 (**2**) and -616758 (**3**) contain the supplemen-

Table 2. Crystal data and refinement details for the complexes.

	1a	**1b**	**2**	**3**
Empirical formula	$C_{33}H_{37}Cl_3Ni_2N_8$, 2 CH_3OH	$C_{34}H_{41}ClNi_2N_8O^{2+}$, 2 ClO_4^-	$C_{21}H_{31}Cl_3Ni_2N_6O_2$, H_2O	$C_{31}H_{37}Cl_2Ni_2N_8O_2^+$, Cl^-, 2 CH_3OH
Formula mass	833.56	929.52	641.30	841.54
Crystal size [mm]	0.45 × 0.35 × 0.29	0.34 × 0.22 × 0.18	0.31 × 0.25 × 0.19	0.44 × 0.28 × 0.15
Crystal system	monoclinic	monoclinic	monoclinic	monoclinic
Space group	$P2_1/n$ (No. 14)	$P2_1/c$ (No. 14)	$C2/m$ (No. 12)	$P2_1/n$ (No. 14)
a [Å]	14.345(2)	17.8241(14)	14.6945(9)	8.5936(15)
b [Å]	8.4514(14)	9.4017(4)	19.1109(8)	27.578(5)
c [Å]	29.544(5)	24.1439(18)	9.8611(6)	15.743(3)
β [°]	96.637(4)	109.459(6)	112.408(4)	95.329(4)
V [$Å^3$]	3557.7(10)	3814.9(4)	2560.1(2)	3715.0(11)
$\rho_{calcd.}$ [g cm^{-3}]	1.556	1.618	1.664	1.505
Z	4	4	4	4
F(000)	1736	1920	1328	1752
μ [mm^{-1}]	1.330	1.262	1.820	1.278
T_{max}/T_{min}	0.6991/0.5860	0.8078/0.6673	0.7611/0.5666	0.8314/0.6032
hkl range	±18, ±10, –36–38	±20, –9–11, ±28	±17, ±22, –10–11	–9–11, ±35, –12–20
θ range [°]	2.39–27.50	1.79–24.80	1.84–24.83	1.97–27.50
Measured refl.	35288	28730	25635	27111
Unique refl. [R_{int}]	8159 [0.0210]	6502 [0.0776]	2293 [0.0581]	8499 [0.0211]
Observed refl. [$I > 2\sigma(I)$]	7205	4376	2087	7258
Data/restraints/param.	8159–0–461	6502–22–520	2293–1–175	8499–0–471
Goodness-of-fit	1.042	1.008	1.075	1.049
R_1/wR_2 [$I > 2\sigma(I)$]	0.0275–0.0672	0.0439–0.0903	0.0229–0.0620	0.0298–0.0714
R_1/wR_2 (all data)	0.0330–0.0704	0.0740–0.0970	0.0256–0.0631	0.0386–0.0768
Resid. el. dens. [e $Å^{-3}$]	0.466/–0.229	0.813/–0.544	0.407/–0.384	0.682/–0.298

tary crystallographic data for this paper. These data can be obtained free of charge from The Cambridge Crystallographic Data Centre via www.ccdc.cam.ac.uk/data_request/cif.

Supporting Information (see footnote on the first page of this article): ORTEP plots of the molecular structures in Figures S1–S4.

Acknowledgments

We sincerely thank the China Scholarship Council for a postdoctoral fellowship (to F.-M. N.) and Prof. Peter Roesky (FU Berlin) for collecting some of the X-ray data.

[1] A. S. Borovik, *Acc. Chem. Res.* **2005**, *38*, 54–61.
[2] J. C. Mareque Rivas, S. L. Hinchley, L. Metteau, S. Parsons, *Dalton Trans.* **2006**, 2316–2322.
[3] L. Brammer, *Dalton Trans.* **2003**, 3145–3157.
[4] G. P. A. Yap, A. L. Rheingold, P. Das, R. H. Crabtree, *Inorg. Chem.* **1995**, *34*, 3474–3476.
[5] G. Aullón, D. Bellamy, L. Brammer, E. A. Bruton, A. G. Orpen, *Chem. Commun.* **1998**, 653–654.
[6] L. Brammer, E. A. Bruton, P. Sherwood, *New J. Chem.* **1999**, *23*, 965–968.
[7] a) J. C. Mareque Rivas, L. Brammer, *Inorg. Chem.* **1998**, *37*, 4756–4757; b) A. Angeloni, P. C. Craword, A. G. Orpen, T. J. Podesta, B. J. Shore, *Chem. Eur. J.* **2004**, *10*, 3783–3791; c) Y. J. Park, J.-S. Kim, K.-T. Youm, N.-K. Lee, J. Ko, H.-S. Park, M.-J. Jun, *Angew. Chem.* **2006**, *118*, 4396–4400; *Angew. Chem. Int. Ed.* **2006**, *45*, 4290–4294.
[8] a) T. Steiner, *Acta Crystallogr., Sect. B* **1998**, *54*, 456–463; b) T. Steiner, *Angew. Chem.* **2002**, *114*, 50–80.
[9] D.-H. Lee, H. J. Kwon, B. P. Patel, L. M. Liable-Sands, A. L. Rheingold, R. H. Crabtree, *Organometallics* **1999**, *18*, 1615–1621.
[10] J. Ackermann, F. Meyer, H. Pritzkow, *Inorg. Chim. Acta* **2004**, *357*, 3703–3711.
[11] S.-J. Barlow, S. J. Hill, J. E. Hocking, P. Hubberstey, W.-S. Li, *J. Chem. Soc., Dalton Trans.* **1997**, 4701–4703.
[12] B. Bauer-Siebenlist, F. Meyer, E. Farkas, D. Vidovic, S. Dechert, *Chem. Eur. J.* **2005**, *11*, 4349–4360.
[13] J. Ackermann, S. Buchler, F. Meyer, *C. R. Chim.*, in press.
[14] a) F. Meyer, S. Beyreuther, K. Heinze, L. Zsolnai, *Chem. Ber./Recueil* **1997**, *130*, 605–613; b) F. Meyer, K. Heinze, B. Nuber, L. Zsolnai, *J. Chem. Soc., Dalton Trans.* **1998**, 207–213; c) F. Meyer, P. Rutsch, *Chem. Commun.* **1998**, 1037–1038; d) F. Meyer, E. Kaifer, P. Kircher, K. Heinze, H. Pritzkow, *Chem. Eur. J.* **1999**, *5*, 1617–1630; e) J. Ackermann, F. Meyer, E. Kaifer, H. Pritzkow, *Chem. Eur. J.* **2002**, *8*, 247–258; f) S. Buchler, F. Meyer, E. Kaifer, H. Pritzkow, *Inorg. Chim. Acta* **2002**, *337*, 371–386; g) B. Bauer-Siebenlist, F. Meyer, E. Farkas, D. Vidovic, J. A. C. Seijo, R. Herbst-Irmer, H. Pritzkow, *Inorg. Chem.* **2004**, *43*, 4189–4202.
[15] B. Brewer, N. R. Brooks, S. Abdul-Halim, A. G. Sykes, *J. Chem. Crystallogr.* **2003**, *33*, 651–662.
[16] A. E. Oblezov, D. R. Talham, K. A. Abboud, *Acta Crystallogr., Sect. E* **2003**, *59*, m1070–m1071.
[17] a) F. Meyer, U. Ruschewitz, P. Schober, B. Antelmann, L. Zsolnai, *J. Chem. Soc., Dalton Trans.* **1998**, 1181–1186; b) S. Buchler, F. Meyer, A. Jacobi, P. Kirchner, L. Zsolnai, *Z. Naturforsch., B: Chem. Sci.* **1999**, *54b*, 1295–1306.
[18] Simulation of the experimental magnetic data with a full-matrix diagonalization of exchange coupling and Zeeman splitting was performed with the julX program (E. Bill, Max Planck Institute for Bioinorganic Chemistry, Mülheim/Ruhr, Germany).
[19] When the term for zero-field splitting was included in Equation (1), the best fit gave $g = 2.18$, $J = -3.7\ cm^{-1}$, $D = -0.05\ cm^{-1}$, $PI = 1\%$ and $TIP = 7.3 \times 10^{-4}\ cm^3 mol^{-1}$ for **1a** and $g = 2.21$, $J = -1.7\ cm^{-1}$, $D = -0.51\ cm^{-1}$, $PI = 2\%$ and $TIP = 4.3 \times 10^{-4}\ cm^3 mol^{-1}$ for **3**.
[20] G. M. Sheldrick, *SHELXL-97*, *Program for Crystal Structure Refinement*, University of Göttingen, **1997**; G. M. Sheldrick, *SHELXS-97*, *Program for Crystal Structure Solution*, University of Göttingen, **1997**.
[21] G. M. Sheldrick, *SADABS*, *Program for Empirical Absorption Correction of Area Detector Data*, University of Göttingen, **1997**.
[22] STOE & CIE GmbH, *X-RED*, Darmstadt, **2002**.

Received: September 22, 2006
Published Online: February 13, 2007

